Journal of Environmental Chemical Engineering 12 (2024) 112764

Contents lists available at ScienceDirect

Journal of Environmental Chemical Engineering

journal homepage: www.elsevier.com/locate/jece

Process performance and precipitate quality of phosphorus recovery by struvite precipitation in a fluidized bed reactor using a MgO industrial by-product

V.B. Aguilar-Pozo [a,b], J.M. Chimenos [b], S. Peña-Picola [a], K. Olaciregui-Arizmendi [c,d], B. Elduayen-Echave [c,d], E. Ayesa [c,d], S. Astals [a,*]

[a] Department of Chemical Engineering and Analytical Chemistry, University of Barcelona, Barcelona 08028, Spain
[b] Department of Materials Science and Physical Chemistry, University of Barcelona, Barcelona 08028, Spain
[c] CEIT-Basque Research and Technology Alliance (BRTA), Donostia-San Sebastián 20018, Spain
[d] Universidad de Navarra, Tecnun, Donostia-San Sebastián 20018, Spain

ARTICLE INFO

Editor: <>

Keywords:
Anaerobic digestion
Magnesium ammonium phosphate
Magnesium oxide by-product
Phosphorus recovery
Struvite precipitation

ABSTRACT

Phosphorus recovery through struvite precipitation has gained interest due to the potential use of struvite as a fertiliser, with fluidised bed reactors being a popular technology for carrying out the process. Struvite precipitation requires a magnesium source and an alkaline reagent. This research uses a low-grade magnesium oxide (LG-MgO) industrial by-product with a 56 wt% of MgO as magnesium source and an alkaline reagent to lower operating costs and value-add an industrial by-product. LG-MgO is poorly soluble in water, but its solubility increases significantly when dissolved in anaerobic digestion supernatants due to its circumneutral pH and high buffer capacity. Phosphorus precipitation was carried out in a laboratory-scale fluidised bed reactor where three operating variables (i.e. P:Mg molar ratio, feed inlet position, and recirculation flow rate) were studied to determine the LG-MgO impact on precipitate struvite content. Experimental results showed a high struvite content in all precipitates, close to the values reported for pure magnesium sources. The P:Mg molar ratio influenced precipitate composition. The percentage of struvite in the precipitate were 75–82 wt%, 85–88 wt%, and 75–76 wt% for the P:Mg ratio of 1:0.5, 1:1 and 1:3, respectively. The feed inlet position (side or bottom) also had an impact on precipitate struvite content when the P:Mg molar ratio was 1:3, but not for the other molar ratios. The recirculation flow rate did not have a significant impact on precipitate struvite content.

1. Introduction

Phosphorus is a limited resource and an essential nutrient for life [1]. Phosphorus rocks reserves are unevenly distributed worldwide since nearly 75 % of the global reserves are located in China, Morocco, the United States of America and Russia [1,2]. Every year, phosphorus consumption is increasing, and phosphorus reserves are being depleted to satisfy this demand [1]. Furthermore, the expenses associated with extraction, processing, and shipping are rising. Consequently, the European Commission (EC) has classified phosphorus as a critical raw material [3]. This designation acknowledges the critical role that phosphorus in our society and highlights the importance of strategic management and sustainable practices to ensure its availability and mitigate potential supply chain risks. Scarcity is not the only problem associated with phosphorus. Phosphorus and nitrogen discharges into aquatic ecosystems contribute to eutrophication [4]. Accordingly, the Council Directive 91/271/CEE on urban wastewater treatments requires the removal of phosphorus and nitrogen when discharges are directed towards environmentally sensitive areas [5]. One potential solution to address the rapid depletion of phosphorus is its recovery in wastewater treatment plants (WWTPs). The most common phosphorus removal processes in WWTPs are chemical precipitation using iron and aluminium salts, enhanced biological phosphorus removal and struvite precipitation [6]. Struvite precipitation could satisfy 15–20 % of the EU phosphorus demand while reducing its concentration in the WWTP discharge and obtaining a product with potential commercial value [7].

In recent years, controlled precipitation of phosphates as struvite has gained interest as a phosphorus recovery technology in WWTPs and its

* Corresponding author.
E-mail address: sastals@ub.edu (S. Astals).

https://doi.org/10.1016/j.jece.2024.112764
Received 17 November 2023; Received in revised form 6 March 2024; Accepted 9 April 2024
Available online 14 April 2024

potential use as slow-release fertiliser. Additionally, controlled precipitation can also mitigate unwanted precipitation issues within pipes and elbows in the WWTPs, further enhancing its applicability by reducing operation and maintenance costs [6,8]. Today, about 15,000 t·year^{-1} of struvite are produced at WWTPs in Europe [9]. Struvite is a crystalline mineral composed of magnesium, ammonium and phosphate ($MgNH_4PO_4{\cdot}6H_2O$) in an equimolar ratio [8]. Struvite precipitation in wastewater requires the addition of magnesium sources (usually $MgCl_2$, $MgSO_4$, MgO, or $Mg(OH)_2$) due to its relatively low concentration compared to ammonium and phosphate ions [10,11]. Adnan et al. [12] studied the effect of P:Mg molar ratios and reported unfavourable phosphorus recovery when P:Mg molar ratios were higher than unity as magnesium availability limited the process. Struvite precipitation is also strongly influenced by pH since struvite solubility decreases with increasing pH, thereby increasing the potential for precipitation [13]. The pH range of struvite precipitation is between 8.0 and 10.7 [14]. However, pH values above 9.0 can favour ammonia nitrogen stripping, i.e. loss of nitrogen in the form of ammonia gas [15]. Accordingly, the preferred working pH range for struvite precipitation is between 8.0 and 9.0 [16]. This pH range is obtained by adding alkaline chemicals (e.g. NaOH) to the reactor or by stripping CO_2 with air [8]. The costs associated with purchasing a magnesium source and an alkali reagent represent 75 % of the struvite precipitation operating cost [1].

To overcome the high costs associated with magnesium sources and alkali reagents, this study explored a low-grade magnesium oxide (LG-MgO) industrial by-product from the calcination process of natural magnesite. LG-MgO is a low-cost by-product (~100 €/t) that can reduce operating costs while value-adding an industrial by-product. LG-MgO contains around 50–65 wt% of MgO as well as other magnesium and calcium minerals, mainly carbonates [17,18]. LG-MgO can serve a dual purpose as both a magnesium source and an alkali reagent for struvite precipitation, allowing for cost savings and improved sustainability and circularity [15,18–21]. Chimenos et al. [20] demonstrated the use of LG-MgO as a magnesium source for the recovery of phosphate as struvite from wastewater generated during the cochineal extraction process. Subsequently, Quintana et al. [18] and Aguilar-Pozo et al. [15] studied struvite precipitation from anaerobic digestion supernatants using LG-MgO in batch experiments. Quintana et al. [18] achieved a phosphorus recovery of 90 % with a pH of 8.6 after 240 min, employing a P:Mg molar ratio of 1:2.5. Aguilar-Pozo et al. [15], who investigated three different LG-MgO, found that a P:Mg molar ratio of 1:1 and 1:2 favoured struvite precipitation over calcium precipitates. Aguilar-Pozo et al. [15] also reported that the percentage of phosphate precipitated varied depending on the LG-MgO reactivity, ranging from 53 % to 72 % and from 89 % to 97 % after 70 min for a P:Mg molar ratio of 1:1 and 1:2, respectively.

Struvite precipitation technologies can be classified into two main categories: fluidised bed reactor (FBR) and continuous stirred tank reactor (CSTR) [22]. FBR is a widely implemented technology for struvite precipitation at WWTPs [16,23], with successful studies available at laboratory, pilot and full scale [4,12,24,25]. The most implemented FBR technologies at industrial scale are OSTARA, PHOSNIX, and MULTIFORM™ [9,22,26]. OSTARA recovers up to 95 % of phosphorus using $MgCl_2$ at a P:Mg molar ratio of 1:1 and NaOH. PHOSNIX recovers more than 90 % of the phosphorus using $Mg(OH)_2$ at P:Mg molar ratio of 1:1 and controlling the pH at 8.2–8.8 using air stripping and NaOH. MULTIFORM™ recovers about 90 % of the phosphorus using $MgCl_2$ at P:Mg molar ratio 1:1 and NaOH. Adnan et al. [12], who studied struvite precipitation using two pilot-scale FBRs, reported phosphorus recovery rates above 90 % using $MgCl_2$ as magnesium source and a pH of 7.3–8.6. Crutchik et al. [24], who used a commercial-grade MgO (80.5 wt% MgO) and two molar P:Mg ratios (i.e. 1:7 and 1:1.5) in a 125 L FBR, showed that struvite content of the precipitate depended on the size of the particles. Specifically, the struvite content was 64 wt% and 78 wt% in the largest precipitates and fine precipitates, respectively. Crutchik et al. [24] also observed that the efficiency of phosphorus recovery was directly dependent on phosphate concentration and pH value and stated that the optimal pH range for effective phosphorus precipitation was between 8.3 and 8.4. Ghosh et al. [27] showed that phosphorus recovery was higher at up-flow rate of 20 cm·min^{-1} than at 40 or 60 cm·min^{-1} due to higher hydraulic retention time (HRT) and reaction time. Currently, there are no studies on the impact of the feed inlet position on process performance although it directly affects the contact between the feed and the magnesium source.

The main goal of this research was to determine the impact of three operating variables on phosphorous recovery and precipitate struvite content when using a LG-MgO as a magnesium source and an alkaline reagent in a fluidised bed reactor. The operating variables under study were (i) P:Mg molar ratio, (ii) feed inlet position into the reactor, and (iii) recirculation flow rate. To the best of the authors' knowledge, this study represents the first laboratory-scale investigation into the utilization of LG-MgO in a fluidised bed reactor for struvite precipitation. The study aims to generate fundamental knowledge of the process to support future utilisation of this by-product in industrial applications.

2. Materials and methods

2.1. Synthetic supernatant and by-product of magnesium oxides

The synthetic supernatant was prepared using deionised water, dipotassium hydrogen phosphate (K_2HPO_4, PanReac AppliChem), and ammonium chloride (NH_4Cl, 99.8 %, PanReac AppliChem). The concentrations in the solution were 80 mg·L^{-1} of PO_4-P and 600 mg·L^{-1} of NH_4-N. The PO_4^{3-} and NH_4^+ ion concentrations were similar to the concentrations reported for full-scale anaerobic digestion supernatants [5]. The initial pH of the synthetic solution was 7.3. Calcium was not added to the synthetic supernatant since the study wanted to study the percentage of impurities in the precipitate when using LG-MgO as a magnesium source. Accordingly, the only calcium source in the reaction medium was the one present in the LG-MgO.

LG-MgO used as a magnesium source was supplied by the company Magnesitas Navarras, S.A. (Navarra, Spain). LG-MgO was obtained in the cyclones and fabric filters from the natural magnesite calcination process. In the rotary kiln, the fine particles were dragged by flue gases to cyclones throughout the combustion process. These particles had a shorter residence time in the kiln, and therefore, part of the magnesite did not complete the calcination process. The LG-MgO used in this study was the one that showed higher phosphorous recovery yields in our previous publication, namely LG-MgO_A [15]. The LG-MgO has a mean diameter (d_{50}) of 12 μm and a medium reactivity, according to the citric acid reactivity test [15,28]. Its composition was estimated by combining the X-ray fluorescence (XRF), X-ray diffraction (XRD) and thermogravimetric analysis (TGA) techniques as described in Aguilar-Pozo et al. [15]. LG-MgO composition was 56.0 wt% MgO, 12.0 wt% $MgCO_3$, 11.6 wt% $CaCO_3$, 8.55 wt% $CaMg(CO_3)_2$, 3.75 wt% $Mg(OH)_2$, 2.24 wt% $Ca(OH)_2$, and small amounts of Al_2O_3, Fe_2O_3, $MgSO_4$, and SiO_2. Aguilar-Pozo et al. [15] conducted a comprehensive characterisation of the LG-MgO used in this study, providing detailed information about its chemical and physical properties.

2.2. Analytical methods

To monitor the struvite precipitation in the FBR, discrete aliquots of the liquid phase were periodically sampled over the course of the experiments. The aliquots were immediately filtered through a 0.45 μm regenerated cellulose syringe filter. Each sample was analysed by duplicate. pH was measured with a micro pH electrode PHEL-GB3–001 connected to a MultiMeter MM41 (Crison). Anion (PO_4-P) and cation (Mg^{2+}, Ca^{2+}, NH_4-N) were measured using an ionic chromatographer 861 Advanced Compact IC Metrohm equipped with Metrosep columns (Metrosep C 2–150/4.0 and Metrosep A Supp 17–250/4.0, respectively).

The precipitated solids were dried at 35 °C for subsequent

characterisation. TGA was conducted using an SDT Q600 Simultaneous TGA204 DSC (TA Instruments) under an inert N_2 gas atmosphere. The analysis involved a heating rate of 10 °C·min^{-1}, and a temperature range from 30 to 1200 °C. TGA analysis facilitated the determination of weight loss percentage and quantification of each mineral phase contained in the precipitated solid. XRF using a Philips PW2400 sequential wavelength-dispersive X-ray fluorescence spectrophotometer was used for elemental analysis of solid phases after calcination at 1050 °C. XRD using a Bragg-Brentano PANalytical X'Pert PRO MPD alpha1 powder diffractometer with Cu$K_{\alpha1}$ radiation ($\lambda = 1.5406$ Å) was used to identify the crystalline mineral phases of the precipitated solid. Fourier-transform infrared spectroscopy by attenuated total reflection (FT-IR ATR) was conducted to compare the molecular geometry of the precipitated solid at different temperatures using a Spectrum Two™ Perkin Elmer spectrometer (range of 4000–400 cm^{-1}, resolution of 4 cm^{-1}). Scanning electron microscopy (SEM) using a Quanta 200 FEI scanning electron microscope combined with X-ray energy dispersive spectroscopy (EDS) was used to show the morphology of the precipitate and the elemental composition of targeted spots. Particle size distribution (PSD) was determined using a LS 13 320 Beckman Coulter laser diffraction particle 207 size analyser.

The composition of the precipitates was obtained by (i) identification of the phases by XRD, (ii) quantification of thermal decomposition products by TGA, (iii) identification of the decomposition reactions and (iv) quantification of the total oxides in the calcined precipitate by XRF, where the percentage of oxides in the precipitate is the difference between the percentage of total oxide and the percentage of oxide in each phase upon decomposition.

2.3. Experimental set-up

The struvite precipitation experiments were carried out in a laboratory-scale FBR. The glass reactor was designed with two sections of increasing diameter (i) the reaction section has a height of 48.2 cm and an internal diameter of 11.0 cm, and (ii) the clarifier section has a height of 13.0 cm and an internal diameter of 17.0 cm. The FBR has three sampling points (named 1, 2 and 3), and two nozzles (side and bottom) with an internal diameter of 2.0 cm (Fig. 1). The difference in diameter between the two sections changes the up-flow velocity, i.e. in the section with a larger diameter the up-flow velocity decreases, resulting in less particles loss in the effluent. The working volume was 4.89 L and the HRT was fixed at 2.5 hours. Two peristaltic pumps were used, one to feed the reactor and another to control the recirculation flow rate.

A total of 12 experiments were carried out to assess the impact of four different configurations (Fig. 1) and three different P:Mg molar ratios on phosphorus recovery and precipitate struvite content. Specifically, the study variables were (i) three P:Mg molar ratios (i.e. 1:0.5, 1:1, and 1:3), with magnesium concentrations calculated from LG-MgO composition, (ii) two feed positions (side and bottom), and (iii) two recirculation flow rates (216 and 907 mL·min^{-1}). The 216 mL·min^{-1} was the minimum flow rate to fluidise the LG-MgO particles, while the 907 mL·min^{-1} recirculation flow rate was the maximum flow rate provided by the peristaltic pump.

The procedure for all experiments was as follows: (i) the total amount of LG-MgO needed for the experiment was added into the recirculation tube in powder, where the amount added was proportional to the total amount of phosphorus during the entire experiment and the targeted P:Mg molar ratio, (ii) reactor filling with the synthetic supernatant, (iii) start-up of the recirculation pump, which added the LG-MgO into fluidised zone of the reactor, (iv) start-up of the feed pump (t = 0), (v) withdrawing 4 mL aliquots at 0, 30, 60, 120, 180, 240, and 300 minutes at the 3 sampling points (bottom, middle, top), (vi) after 300 min the pumps were stopped, (vii) the reactor was emptied and the precipitated solid was collected from the bottom of the reactor. The precipitate was dried at 35 °C (> 24 h) and subsequently characterised as described in Section 2.2. Table 1 shows the initial conditions of each experiment.

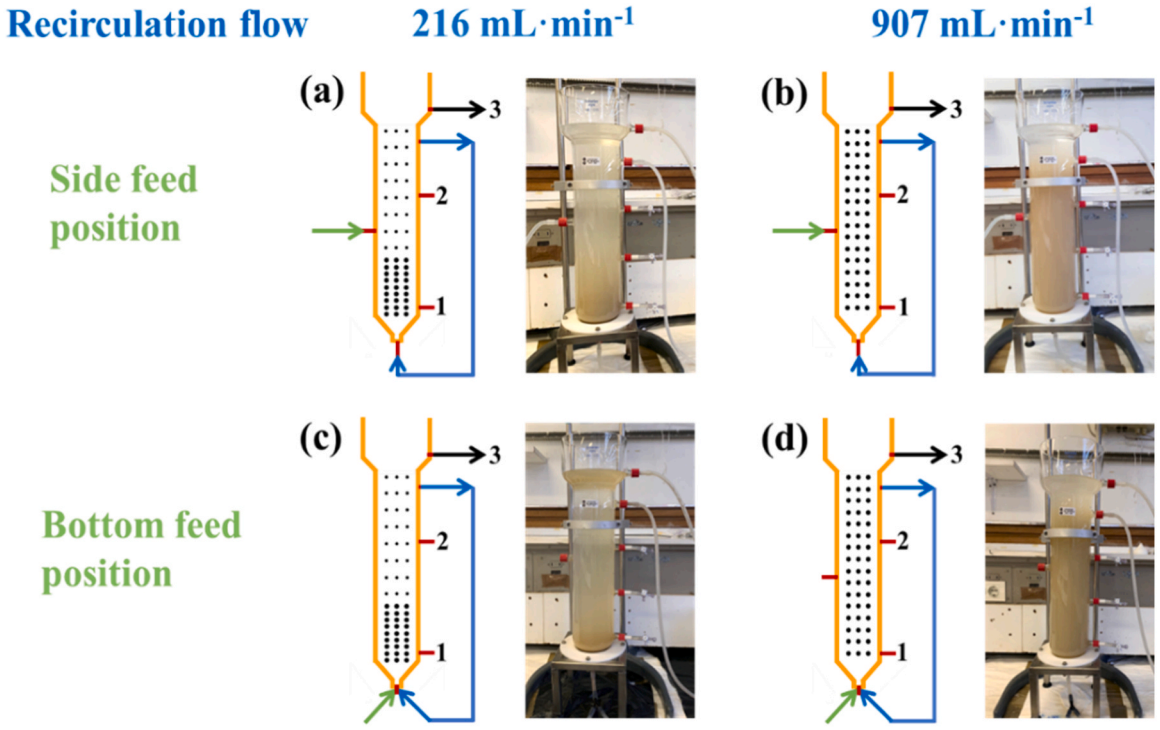

Fig. 1. Configurations used for phosphorus precipitation, each tested at three P:Mg molar ratios (1:0.5, 1:1, and 1:3): (a) side feed position and recirculation flow rate of 216 mL·min^{-1}, (b) side feed position and recirculation flow rate of 907 mL·min^{-1}, (c) bottom feed position and recirculation flow rate of 216 mL·min^{-1}, and (d) bottom feed position and recirculation flow rate of 907 mL·min^{-1}. The three sampling points are (1) bottom, (2) middle and (3) top.

Table 1
Initial conditions of the 12 experiments.

N°	Feed inlet position	Molar Ratio (P:Mg)	Recirculation flow rate ($mL{\cdot}min^{-1}$)	Feed flow rate ($mL{\cdot}min^{-1}$)
1	Side	1:0.5	216	32.6
2	Side	1:0.5	907	32.6
3	Bottom	1:0.5	216	32.6
4	Bottom	1:0.5	907	32.6
5	Side	1:1	216	32.6
6	Side	1:1	907	32.6
7	Bottom	1:1	216	32.6
8	Bottom	1:1	907	32.6
9	Side	1:3	216	32.6
10	Side	1:3	907	32.6
11	Bottom	1:3	216	32.6
12	Bottom	1:3	907	32.6

2.4. Calculations and statistical analysis

The composition of the precipitates obtained in each experiment was estimated through the utilization of various analytical techniques (i.e. XRD, TGA, XRF, and FT-IR) as described in Aguilar-Pozo et al. [15]. Briefly, X-ray diffraction (XRD) results facilitated the identification of the mineral phases present in the precipitates. TGA results allowed the quantification of the percentage of each mineral phase by observing the weight losses attributed to thermal decomposition. The composition was complemented with XRF results, which provides the elemental composition of the sample expressed as its most stable oxide.

Statistical tests were performed to determine whether (i) P:Mg molar ratio (ii) feed position and/or (iii) recirculation flow rate had a significant impact on precipitate struvite content. An analysis of variance (ANOVA) was done using R software (v4.0.3). The confidence level used for the statistical test was 95 % ($\alpha = 0.05$). Four ANOVA tests were carried out, three to evaluate the effects of feed position and recirculation flow rate (independent variables) on precipitate struvite content (dependent variable) for each P:Mg molar ratio (1:0.5, 1:1, and 1:3), and a fourth to evaluate the effect of the P:Mg molar ratio on precipitate struvite content.

3. Results and discussion

3.1. Phosphorus precipitation

The experiments carried out with a P:Mg molar ratio of 1:0.5 and 1:1 showed similar magnesium and phosphorus concentrations and pH values in the three sampling points (Fig. A1 and A2 in the supplementary material). The experiments using a P:Mg molar ratio of 1:3 showed a distinct concentration pattern, with the 1st (bottom) and 2nd (middle) sampling points showing similar values and the 3rd sampling point (top) showing lower values (Fig. A3 in the supplementary material). This divergence could be attributed to two factors: (i) a longer reaction time and path between the 1st and 2nd sampling points before reaching the top section of the reactor, leading to prolonged contact between Mg^{2+}, NH_4^+, and PO_4^{3-} to form struvite and therefore decreasing their concentrations, and (ii) a lower number of LG-MgO particles in the top section of the reactor due to the decreased axial velocity that lowers the release of Mg^{2+} and hydroxide (OH^-) ions from the LG-MgO particles. It is worth noting that for all molar ratios the sedimentation of LG-MgO particles and associated OH^- dissolution at the bottom of the reactors resulted in slightly higher pH values at the 1st sampling point, particularly when the feeding was from the side.

Fig. 2 shows the phosphorus and magnesium concentrations and pH of the FBR effluent (3rd sampling point) of the 12 experiments. The experiments carried out with a P:Mg molar ratio of 1:0.5 and 1:1 showed a consistent and progressive loss of phosphorus through the effluent,

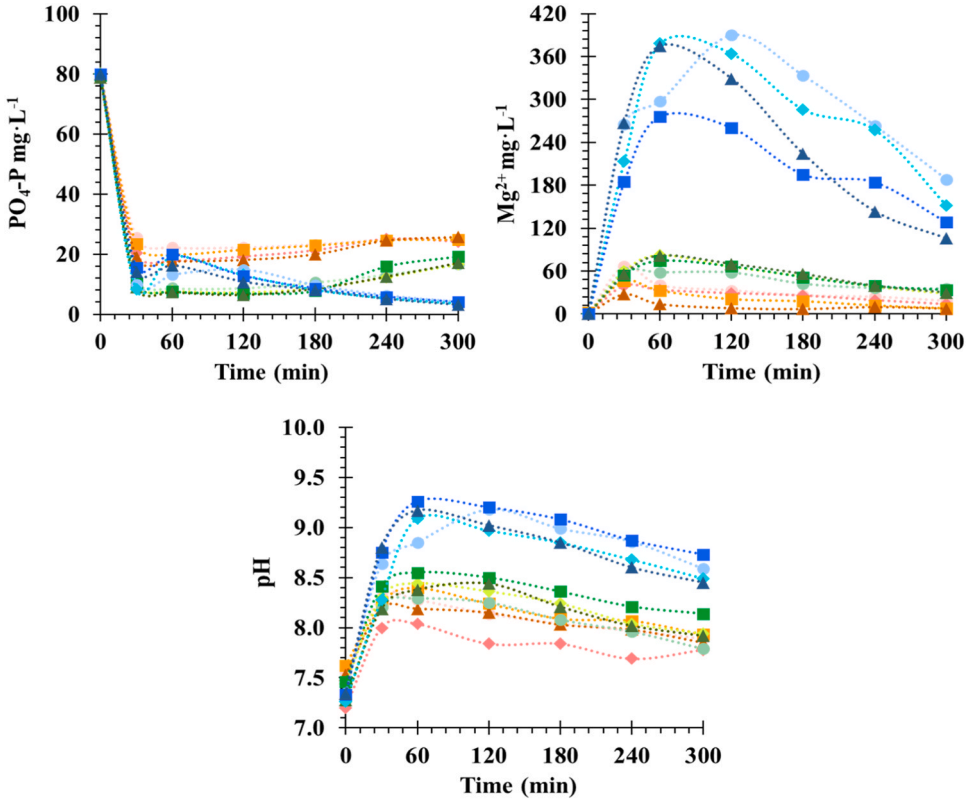

Fig. 2. Phosphorus and magnesium concentrations and pH of the FBR effluent (3rd sampling point). Experiments number: 1 (), 2 (), 3 (), 4 (), 5 (), 6 (), 7 (), 8 (), 9 (), 10 (), 11 (), and 12 ().

with the highest losses occurring at the end of the experiments. The phosphorus concentration in the effluent increased at the end of experiments due to the decrease in Mg^{2+} concentration and pH in the medium (Fig. 2), disfavouring the oversaturation conditions required for struvite precipitation. The experiments carried out at a P:Mg molar ratio of 1:0.5 reached effluent phosphorus concentration below 20 mg·L^{-1} for about 90 min (between minute 30 and 120), then the concentration increased up to 26 mg·L^{-1}. In the experiments with a P:Mg molar ratio of 1:1, the phosphorus concentration remained constant between minute 30 and 180 at about 11 mg PO_4-P·L^{-1}, then the concentration increased up to 18 mg·L^{-1}. The experiments with a P:Mg molar ratio of 1:3 showed the highest reduction in phosphorus after 180 min, reaching concentrations of 3–4 mg PO_4-P·L^{-1} due to the excess of magnesium and the higher pH values (8.8–9.3).

The Mg^{2+} concentration in the effluent increased at the beginning of the experiments as the LG-MgO particles dissolved, then decreased due to (i) losses through the effluent, (ii) dilution of the reaction medium by the feed, and (iii) struvite precipitation (Fig. 2). In the P:Mg molar ratio 1:0.5 experiments, the Mg^{2+} concentration increased up to 56 mg·L^{-1} during the first 30 minutes. Subsequently, the Mg^{2+} concentration decreased but did not reach 0 mg·L^{-1}, even though the amount of LG-MgO added was half the amount required for complete phosphorus precipitation as struvite (Fig. 2). These results suggest that a P:Mg molar ratio of 1:0.5 did not provide favourable conditions for struvite precipitation. The loss of magnesium through the effluent during the experiments can be attributed to several factors. Firstly, the incomplete precipitation of phosphorus with magnesium and ammonium. Secondly, the retention time of magnesium in the reactor (HRT = 2.5 hours) and the continuous dilution of magnesium by the feed. Lastly, the dissolution rate of LG-MgO itself decreased over time due to the lower concentration of MgO and lower reactivity of $MgCO_3$ and $CaMg(CO_3)_2$ in the LG-MgO. In the P:Mg molar ratio 1:1 experiments, Mg^{2+} concentrations reached 82 mg·L^{-1} after the first 60 minutes. Then, the Mg^{2+} concentration decreased, stabilising at values close to 30 mg·L^{-1} (Fig. 2). The experiments with a P:Mg molar ratio of 1:3 resulted in the highest Mg^{2+} concentrations in the effluent. Significant losses of magnesium were observed between the 60 and 120 minute interval, when the effluent had Mg^{2+} concentrations of 375–390 mg·L^{-1}. Despite a gradual decrease in Mg^{2+} concentration, significant losses of magnesium were observed until the end of the experiment. Adding the entire amount of LG-MgO at the beginning of the experiment resulted in the fast dissolution of LG-MgO particles, reducing the LG-MgO surface area and the number of LG-MgO particles. As a result, more magnesium was released than was required for struvite precipitation.

Experiments with the same molar ratio but different configurations showed similar results regardless of the feed inlet position (side or bottom) and recirculation flow rate (216 or 907 mL·min^{-1}). Experiment 11 (bottom feed position and a low recirculation flow rate) had a lower Mg^{2+} concentration in the effluent compared to the other experiments carried out with a P:Mg molar ratio of 1:3 (experiments 9, 10, and 12). In experiment 11, the feed came into direct contact with the LG-MgO particles due to the predominance of fluidisation in the bottom section of the reactor at low recirculation rates. Under these specific conditions, the reaction parameters are primarily controlled by the solubility equilibrium of $Mg(OH)_2$ [29].

pH plays an important role in struvite precipitation as it limits the availability of ammonium ions required for struvite formation, affects the acid-base equilibrium for the protonation of different phosphate species, and controls the liberation of magnesium from the LG-MgO. Struvite reaction can use different phosphate species (Eq. (1)), where *n* can be 0, 1, or 2 [30,31]. In these experiments, the predominant phosphate species in the supernatant were $H_2PO_4^-$ and HPO_4^{2-} as the initial pH was 7.2–7.5. However, pH increased and shifted the equilibrium of the two protonated phosphate species ($H_2PO_4^-$ and HPO_4^{2-}) towards the formation of PO_4^{3-} and the precipitation of struvite. Thus, maintaining an appropriate pH value is essential for facilitating the struvite precipitation process and efficient phosphorus removal.

$$Mg^{2+} + NH_4^+ + H_nPO_4^{n-3} + 6\ H_2O \leftrightarrow MgNH_4PO_4{\cdot}6H_2O + n\ H^+ \quad (1)$$

Fig. 2 shows the pH values of each experiment. The experiments carried out with a P:Mg molar ratio of 1:0.5 and 1:1 showed similar pH values between 7.8 and 8.5, starting from a pH value of about 7.4. However, when the P:Mg molar ratio was 1:3, pH values above 9.0 were reached, followed by a gradual decrease to 8.5–8.7. Generally, the side feed position and low recirculation rate configuration (experiments 1, 5 and 9) showed a lower reduction in phosphorus concentrations, this could imply slightly lower struvite precipitation than the other configurations with the same P:Mg molar ratio.

3.2. Composition of the precipitates

Fig. 3 shows the XRD diffractograms of the solid fraction collected from the 12 experiments, categorised into three groups based on the P:Mg molar ratio of the experiment. All of the precipitates had several mineral phases, including struvite ($MgNH_4PO_4{\cdot}6H_2O$), periclase (MgO), magnesite ($MgCO_3$), dolomite ($CaMg(CO_3)_2$), calcite ($CaCO_3$), and silica (SiO_2). The highest intensity peaks were attributed to struvite, indicating that struvite was the predominant phase in all precipitates. The presence of other mineral phases such as MgO, $MgCO_3$, $CaCO_3$, $CaMg(CO_3)_2$, and SiO_2 can be attributed to the unreacted phases initially present in the LG-MgO used as a magnesium source. These less reactive mineral phases were not fully consumed or dissolved during the precipitation process and remained in the final solid precipitates. It should be considered that LG-MgO is sparingly soluble in deionised water as MgO [32]. However, LG-MgO is more soluble in anaerobic digestion

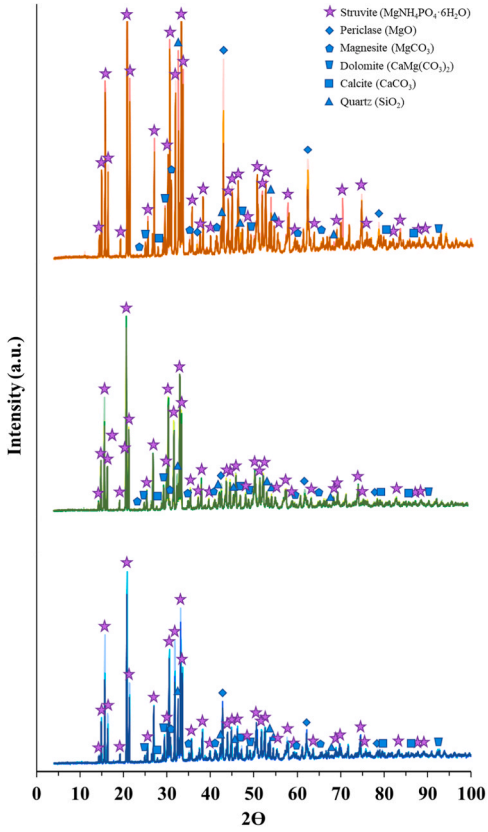

Fig. 3. X-ray diffractograms of the 12 precipitates. P:Mg molar ratio of 1:0.5 [top, experiments: 1 (●), 2 (◆), 3 (■), 4 (▲)], 1:1 [middle, experiments: 5 (●), 6 (◆), 7 (■), 8 (▲)], and 1:3 [bottom, experiments: 9 (●), 10 (◆), 11 (■), 12 (▲)].

supernatants due to its high buffer capacity [15,32]. The solubility of LG-MgO has not been studied, but studies on MgO indicate an enhanced solubility in the presence of protons [32–34], as is the case of anaerobic digestion supernatants [4,32].

The TGA curves of the precipitates show the mass loss steps as a function of temperature. The 12 precipitates displayed similar mass loss steps (Fig. B1 in the supplementary material). As an example, Fig. 4 shows the TGA curve of the precipitate obtained in experiment 1.

The steps observed in the TGA curves correspond to the thermal decomposition of the phases $MgNH_4PO_4{\cdot}6H_2O$, $Mg(OH)_2$, $MgCO_3$, $CaMg(CO_3)_2$ and $CaCO_3$. The thermal decomposition reactions of $Mg(OH)_2$, $MgCO_3$, $CaMg(CO_3)_2$ and $CaCO_3$ are known (Eqs. 2–5).

$$Mg(OH)_2(s) \rightarrow MgO(s) + H_2O(g) \quad (2)$$

$$MgCO_3(s) \rightarrow MgO(s) + CO_2(g) \quad (3)$$

$$CaMg(CO_3)_2(s) \rightarrow MgO(s) + CaO(s) + 2\ CO_2(g) \quad (4)$$

$$CaCO_3(s) \rightarrow CaO(s) + CO_2(g) \quad (5)$$

Bhuiyan et al. [35] and Chen et al. [36] studied the thermal decomposition reactions of struvite and reported the following equations (Eqs. 6–9)).

$$MgNH_4PO_4{\cdot}6H_2O(s) \rightarrow MgNH_4PO_4{\cdot}H_2O(s) + 5\ H_2O(g) \quad (6)$$

$$MgNH_4PO_4{\cdot}6H_2O(s) \rightarrow MgHPO_4{\cdot}3H_2O(s) + 3\ H_2O(g) + NH_3(g) \quad (7)$$

$$MgNH_4PO_4{\cdot}6H_2O(s) \rightarrow MgHPO_4(s) + 6\ H_2O(g) + NH_3(g) \quad (8)$$

$$2\ MgHPO_4(s) \rightarrow MgP_2O_7(s) + H_2O(g) \quad (9)$$

The determination of the struvite decomposition reaction was carried out using FT-IR. Fig. 5 presents the FT-IR spectra of the precipitate and the products of its decomposition at three different temperatures (i.e. 100, 450, and 750 °C). The spectrum at room temperature showed NH_4^+, H_2O, HPO_4^{2-}, and PO_4^{3-} bands, which appear at the frequency ranges of 1149–1493, 1494–1710, 904–1138, and 798–904 cm^{-1}, respectively [36,37]. Even at 100 °C, the NH_4^+, H_2O, HPO_4^{2-}, and PO_4^{3-} bands were still present in the spectra, indicating that struvite at 100 °C does not completely decompose. The presence of NH_4^+ and H_2O bands indicated that the loss of the two compounds was gradual. The spectra at 450 and 750 °C showed a shift in the 1494–1710, 904–1138 cm^{-1} bands and a new formation of the P-O-P stretching vibrations at 699–816 cm^{-1}, corresponding to the P_2O_7 [36]. These results indicated that the struvite decomposition reaction took place as described in Eq. (10). Importantly, the percentage of P_2O_7 obtained by XRF (Table A1 in the supplementary material) and the value calculated through the TGA results were similar,

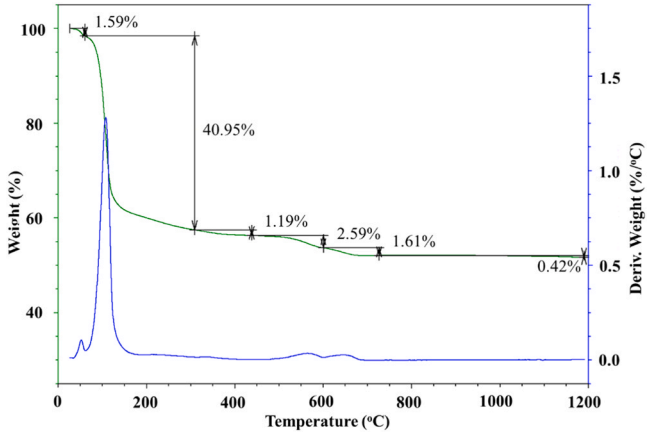

Fig. 4. TGA diffractogram of the precipitate obtained in experiment 1. Mass loss steps versus temperature (green line) and derivative of weight versus temperature (blue line).

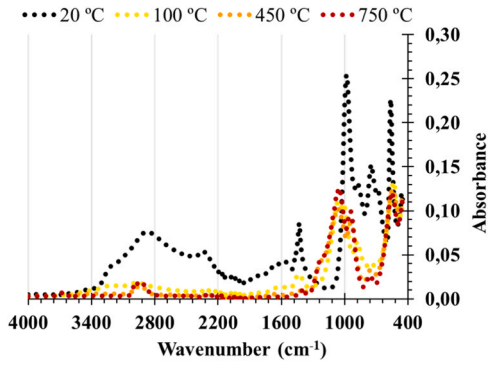

Fig. 5. FT-IR spectra of the precipitated solid at 20 °C and the products of its decomposition at temperatures of 100, 450 and 750 °C.

indicating that Eq. (10) accurately describes struvite thermal decomposition.

$$2\ MgNH_4PO_4{\cdot}6H_2O(s) \rightarrow Mg_2P_2O_7(s) + 13\ H_2O(g) + 2\ NH_3(g) \quad (10)$$

Table 2 presents the percentage of each phase according to the TGA results and using the following reactions (Eqs. 2–5 and 10). The thermal decomposition of struvite involving both ammonia and crystallization water began at about 60 °C and was completed at above 300 °C. Struvite commonly has an orthorhombic crystalline geometry made by an octahedral ($Mg(6H_2O)^{2+}$) and two tetrahedral (NH_4^+ and PO_4^{3-}) groups where H_2O molecules have six short hydrogen bonds, i.e. six stable bonds that help maintain crystal structure [14,38]. The decomposition temperature ranges for $Mg(OH)_2$ (300–450 °C), $MgCO_3$ (450–600 °C), $CaMg(CO_3)_2$ (600–725 °C) and $CaCO_3$ (725–1200 °C) are consistent with the values reported by Giro-Paloma et al. [17].

Table 3 shows the mineral composition of the 12 precipitates. As indicated by the XRD diffractograms (Fig. 3) and the mass loss in the TGA curves (Table 2), struvite was the main phase in all precipitates. The precipitates from the experiments carried out with a P:Mg molar ratio of 1:1 (experiment 5, 6, 7 and 8) had the highest struvite content, with a percentage of 85.3–88.2 wt%. This was followed by the molar ratios of 1:0.5 and 1:3, which resulted in a struvite content of 75.1–82.4 wt% and 74.7–76.4 wt%, respectively. The struvite content reported in the precipitates using $Mg(OH)_2$ and $MgCl_2$ is 78.0 and 80.0–93.5 wt%, respectively [4,12,24]. These percentages are not far from the values obtained using an industrial LG-MgO by-product. These results demonstrate that LG-MgO holds potential as both a magnesium source and an alkali reagent for struvite precipitation, offering potential cost savings, as its cost is ~100 €·t^{-1} [15] compares favourably with $MgCl_2$ and NaOH, which are priced at 370 and 620 €·t^{-1} [39],

Table 2
The decomposition temperature range and weight percentage loss of the main mineral phases present in the 12 precipitates.

Mineral phase (wt%)	$MgNH_4PO_4{\cdot}6(H_2O)$	$Mg(OH)_2$	$MgCO_3$	$CaMg(CO_3)_2$	$CaCO_3$
Temperature (°C)	60–300	300–450	450–600	600–725	725–1200
1	40.95	1.19	2.59	1.61	0.42
2	46.22	1.56	2.33	1.43	0.83
3	42.53	1.36	2.63	1.55	0.79
4	45.09	1.12	2.56	1.26	0.43
5	46.61	1.38	2.03	1.13	1.00
6	47.17	1.13	2.05	0.99	0.57
7	49.70	1.34	1.75	0.81	0.80
8	47.43	0.99	1.75	0.74	0.18
9	42.39	1.34	3.24	1.79	0.84
10	40.87	1.59	3.82	2.24	0.98
11	41.66	1.28	3.63	1.93	0.56
12	42.77	2.09	3.73	2.00	1.13

Table 3
Mineral composition (wt%) and mean diameter of the 12 precipitates.

Experiment	1	2	3	4	5	6	7	8	9	10	11	12
$MgNH_4PO_4{\cdot}6(H_2O)$	75.1	82.4	76.0	81.9	85.3	86.3	88.2	86.3	74.7	74.7	76.2	76.4
MgO	5.8	1.9	6.5	2.8	0.8	0.4	0.0	1.2	5.2	2.3	4.2	0.8
$Mg(OH)_2$	3.7	4.5	3.4	2.9	4.0	3.1	3.3	2.4	3.5	4.9	3.5	6.4
$MgCO_3$	5.0	4.5	5.0	4.9	3.9	3.9	2.9	3.4	6.2	7.3	7.0	7.5
$CaMg(CO_3)_2$	3.4	3.0	3.3	2.6	2.4	2.1	1.7	1.6	3.8	4.7	4.0	4.2
$CaCO_3$	1.0	1.9	1.8	1.0	2.3	1.3	1.8	0.4	1.9	2.2	1.3	2.6
$Ca(OH)_2$	0.2	0.6	1.0	0.7	0.5	0.5	0.6	0.8	0.9	0.2	0.6	0.4
SiO_2	1.1	0.7	0.8	0.7	0.6	0.6	0.5	0.6	1.1	1.0	1.0	1.0
Fe_2O_3	0.9	0.8	0.9	0.8	0.7	0.7	0.6	0.6	1.3	1.2	1.2	1.1
H_2O	3.2	0.3	1.9	1.6	0.3	1.3	0.8	2.1	1.9	1.6	1.4	0.4
Mean diameter (μm)	37.5	37.2	26.9	51.1	47.6	32.6	33.0	16.8	14.4	14.4	17.1	16.0

respectively. The precipitates from the experiments carried out with a P:Mg molar ratio of 1:3 had the highest percentage of unreacted mineral phases (i.e. $MgCO_3$, $CaCO_3$, $CaMg(CO_3)_2$, Fe_2O_3 and SiO_2). As a result, the struvite content of the precipitates decreased. These results align with other studies on struvite precipitation that have stated that an excess concentration of magnesium does not positively influence struvite crystallization [40,41]. This is because elevated magnesium concentration and pH can promote magnesium phosphates or/and magnesium carbonates co-precipitation alongside struvite [24]. Finally, it should be noted that the percentage of MgO and $Mg(OH)_2$ in the 12 precipitates were lower than 6.5 and 6.4 wt%, respectively. The Mg^{2+} dissolution from MgO and $Mg(OH)_2$ is quite similar when there are protons in the medium [42]. The low percentage of MgO in the precipitates shows the high dissolution of MgO from the LG-MgO particles during the experiments.

The analysis of variance (ANOVA) showed that the experiments carried out with a P:Mg molar ratio of 1:0.5 and 1:1, the feed position ($P = 0.856$, $P = 0.488$) and the recirculation flow rate ($P = 0.069$, $P = 0.825$) had no significant impact on the percentage of struvite in the precipitate. In the experiments carried out with a P:Mg molar ratio of 1:3, the percentage of struvite in the precipitate was significantly affected by the feed position ($P = 0.037$), but not by the recirculation flow rate ($P = 0.570$). These results are consistent with Tarragó et al. [43] who concluded that phosphorus recovery was not significantly affected by the up-flow velocity. ANOVA results also revealed that the percentage of struvite in the precipitate was significantly influenced by the P:Mg molar ratios ($P = 0.0006$). Overall, ANOVA results provided the following insights: (i) the recirculation flow rate did not significantly affect the struvite content, suggesting that low recirculation flow rates able to maintain solids suspended could be employed to reduce operating costs, (ii) the feed position had an impact on precipitate struvite content, particularly when the P:Mg molar ratio was 1:3, and (iii) the P:

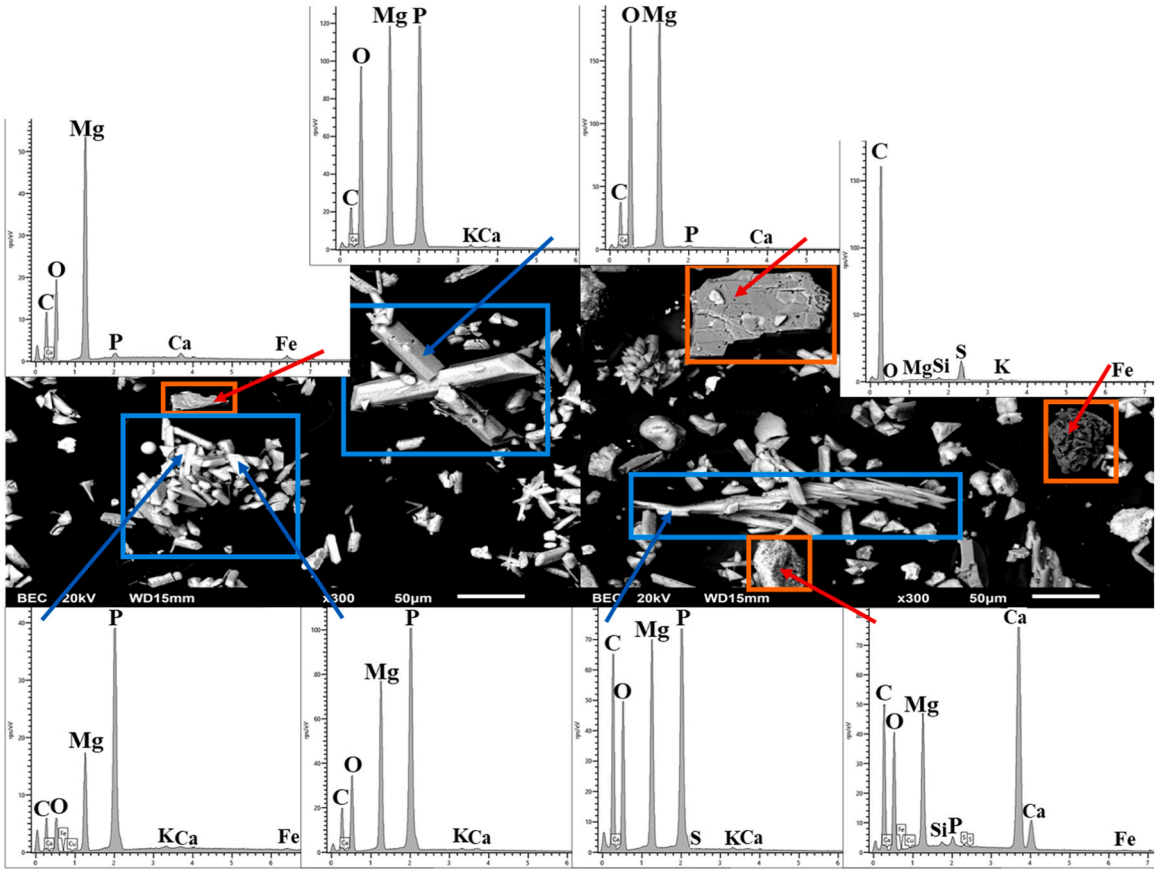

Fig. 6. SEM micrographs and spots (arrows) analysed by EDS of the precipitates obtained in experiments 3 and 6. Blue frame: struvite crystal geometries and orange frame other mineral phases.

Mg molar ratio itself influenced the precipitate struvite content, with the 1:1 ratio demonstrating the highest struvite percentage.

At the end of the experiment (300 min), it was evident that large struvite particles had not been formed (Table 3). Table 3 shows that the smallest particles were obtained when operating with the highest P:Mg molar ratio (1:3). It can be hypothesised that as the amount of LG-MgO increased, the degree of oversaturation increased, which favoured the nucleation stage [30]. This nucleation stage promoted the formation of nuclei or crystal seeds but had no effect on their subsequent growth.

The 12 precipitates had similar morphologies. Fig. 6 shows the different morphologies found in the precipitates and the elemental composition of 8 spots. The struvite geometries depicted in Fig. 6 exhibit the following characteristics: (i) agglomerations of polyhedral shapes, (ii) crystal growth occurring in different directions, and (iii) elongated-prismatic morphology. The formation of polyhedral struvite crystals was reported to be favoured under conditions of lower oversaturation and lower alkaline pH values [44]. SEM micrographs also showed that the majority of the MgO particles present in LG-MgO were dissolved but that certain mineral phases existing in the LG-MgO remained unreacted and were present in the precipitates (e.g. SiO_2 and $CaMg(CO_3)_2$).

4. Conclusions

Experimental results showed that LG-MgO can be used as a magnesium source and an alkali reagent for struvite precipitation, offering potential cost savings compared to $MgCl_2$ and NaOH. The configuration that resulted in the highest phosphorus recovery and struvite content was a P:Mg molar ratio of 1:1, bottom feed into position and high recirculation flow rates. The precipitates obtained from the struvite precipitation in a lab-scale fluidised bed reactor had (i) struvite as the main mineral phase (75–88 wt%) and (ii) low percentages of impurities from LG-MgO. The percentage of struvite in the precipitate was mainly affected by the P:Mg molar ratio. The P:Mg molar ratio of 1:1 showed the highest struvite percentages (85–88 wt%) followed by the molar ratios of 1:0.5 (75–82 wt%) and 1:3 (75–76 wt%). The composition of the precipitate was also influenced by the feed position (side or bottom) for the experiments carried out at a P:Mg molar ratio of 1:3. The recirculation flow rate did not significantly affect the struvite percentage of the precipitates. Using a LG-MgO with 44 wt% of other mineral phases did not result in a struvite-poor precipitate.

CRediT authorship contribution statement

V.B. Aguilar-Pozo: Writing – original draft, Validation, Investigation, Formal analysis. **J.M. Chimenos:** Writing – review & editing, Supervision, Funding acquisition, Conceptualization. **S. Peña-Picola:** Writing – review & editing, Investigation. **K. Olaciregui-Arizmendi:** Writing – review & editing, Validation. **B. Elduayen-Echave:** Writing – review & editing, Validation. **E. Ayesa:** Writing – review & editing, Validation, Funding acquisition. **S. Astals:** Writing – review & editing, Supervision, Methodology, Funding acquisition, Conceptualization.

Declaration of Competing Interest

The authors declare the following financial interests/personal relationships which may be considered as potential competing interests: Sergi Astals Garcia reports financial support was provided by Spain Ministry of Science and Innovation. If there are other authors, they declare that they have no known competing financial interests or personal relationships that could have appeared to influence the work reported in this paper.

Data Availability

Data will be made available on request.

Acknowledgements

This research was supported by the grant RTC2019–007257–5 funded by MCIN/AEI /10.13039/501100011033. Ms. Verónica Aguilar and Mr. Sergi Peña are grateful to grants 2022 FI_B 00032 and 2022 FISDU 00140, respectively funded by The Agència de Gestió d'Ajuts Universitaris i de Recerca (AGAUR) and, as appropriate, by ESF Investing in your future. The Department of Education of the Basque Government contributed through Mr. Kepa Olaciregui's PhD grant (PRE_2023_2_0142). Sergi Astals is thankful to the Spanish Ministry of Science, Innovation and Universities for his Ramon y Cajal fellowship (RYC-2017–22372). The authors would like to thank the Catalan Government for the quality accreditation given to both research groups of the University of Barcelona (2021 SGR 00708 and 2021 SGR 00234). DIOPMA (2021 SGR 00708) is a certified agent TECNIO in the category of technology developers from the Government of Catalonia. The authors are grateful to Magnesitas Navarras S.A. and Navarra de Infraestructuras Locales S.A. for providing LG-MgO sample and research support.

Appendix A. Supporting information

Supplementary data associated with this article can be found in the online version at doi:10.1016/j.jece.2024.112764.

References

[1] L. Peng, H. Dai, Y. Wu, Y. Peng, X. Lu, A comprehensive review of the available media and approaches for phosphorus recovery from wastewater, Water Air Soil Pollut. 229 (2018) 115, https://doi.org/10.1007/s11270-018-3706-4.
[2] D.-J.D. Kok, S. Pande, J.B. van Lier, A.R.C. Ortigara, H. Savenije, S. Uhlenbrook, Global phosphorus recovery from wastewater for agricultural reuse, Hydrol. Earth Syst. Sci. 22 (2018) 5781–5799, https://doi.org/10.5194/hess-22-5781-2018.
[3] EC, Scope Newsletter, (2013). ⟨https://www.phosphorusplatform.eu/2013⟩.
[4] Y.-J. Shih, R.R.M. Abarca, M.D.G. de Luna, Y.-H. Huang, M.-C. Lu, Recovery of phosphorus from synthetic wastewaters by struvite crystallization in a fluidized-bed reactor: Effects of pH, phosphate concentration and coexisting ions, Chemosphere 173 (2017) 466–473, https://doi.org/10.1016/j.chemosphere.2017.01.088.
[5] L. Pastor, D. Mangin, R. Barat, A. Seco, A pilot-scale study of struvite precipitation in a stirred tank reactor: conditions influencing the process, Bioresour. Technol. 99 (2008) 6285–6291, https://doi.org/10.1016/j.biortech.2007.12.003.
[6] P. Achilleos, K.R. Roberts, I.D. Williams, Struvite precipitation within wastewater treatment: a problem or a circular economy opportunity? Heliyon 8 (2022) e09862 https://doi.org/10.1016/j.heliyon.2022.e09862.
[7] L. Peng, H. Dai, Y. Wu, Y. Peng, X. Lu, A comprehensive review of phosphorus recovery from wastewater by crystallization processes, Chemosphere 197 (2018) 768–781, https://doi.org/10.1016/j.chemosphere.2018.01.098.
[8] Y. Ye, H.H. Ngo, W. Guo, Y. Liu, S.W. Chang, D.D. Nguyen, H. Liang, J. Wang, A critical review on ammonium recovery from wastewater for sustainable wastewater management, Bioresour. Technol. 268 (2018) 749–758, https://doi.org/10.1016/j.biortech.2018.07.111.
[9] A. Siciliano, C. Limonti, G.M. Curcio, Advances in Struvite Precipitation Technologies for Nutrients Removal and Recovery from Aqueous Waste and Wastewater, (2020) 36.
[10] S. Kataki, H. West, M. Clarke, D.C. Baruah, Phosphorus recovery as struvite from farm, municipal and industrial waste: feedstock suitability, methods and pre-treatments, Waste Manag. 49 (2016) 437–454, https://doi.org/10.1016/j.wasman.2016.01.003.
[11] N. Marti, A. Bouzas, A. Seco, J. Ferrer, Struvite precipitation assessment in anaerobic digestion processes, Chem. Eng. J. 141 (2008) 67–74, https://doi.org/10.1016/j.cej.2007.10.023.
[12] A. Adnan, D.S. Mavinic, F.A. Koch, Pilot-scale study of phosphorus recovery through struvite crystallization_examining the process feasibility, Environ. Eng. Sci. 2 (2003) 315–324.
[13] A. Kozik, N. Hutnik, K. Piotrowski, A. Matynia, Continuous reaction crystallization of struvite from diluted aqueous solution of phosphate(V) ions in the presence of magnesium ions excess, Chem. Eng. Res. Des. 92 (2014) 481–490, https://doi.org/10.1016/j.cherd.2013.08.032.
[14] J.D. Doyle, S.A. Parsons, Struvite formation, control and recovery, Water Res. 36 (2002) 3925–3940, https://doi.org/10.1016/S0043-1354(02)00126-4.
[15] V.B. Aguilar-Pozo, J.M. Chimenos, B. Elduayen-Echave, K. Olaciregui-Arizmendi, A. López, J. Gómez, M. Guembe, I. García, E. Ayesa, S. Astals, Struvite precipitation in wastewater treatment plants anaerobic digestion supernatants using a magnesium oxide by-product, Sci. Total Environ. 890 (2023) 164084, https://doi.org/10.1016/j.scitotenv.2023.164084.
[16] M. Muys, R. Phukan, G. Brader, A. Samad, M. Moretti, B. Haiden, S. Pluchon, K. Roest, S.E. Vlaeminck, M. Spiller, A systematic comparison of commercially

produced struvite: quantities, qualities and soil-maize phosphorus availability, Sci. Total Environ. 756 (2021) 143726, https://doi.org/10.1016/j.scitotenv.2020.143726.
[17] J. Giro-Paloma, J. Formosa, J.M. Chimenos, Stabilization Study of a Contaminated Soil with Metal(loid)s Adding Different Low-Grade MgO Degrees, (2020) 17.
[18] M. Quintana, M.Fco Colmenarejo, J. Barrera, G. García, E. García, A. Bustos, Use of a byproduct of magnesium oxide production to precipitate phosphorus and nitrogen as struvite from wastewater treatment liquors, J. Agric. Food Chem. 52 (2004) 294–299, https://doi.org/10.1021/jf0303870.
[19] S. Astals, M. Martínez-Martorell, S. Huete-Hernández, V.B. Aguilar-Pozo, J. Dosta, J.M. Chimenos, Nitrogen recovery from pig slurry by struvite precipitation using a low-cost magnesium oxide, Sci. Total Environ. 768 (2021) 144284, https://doi.org/10.1016/j.scitotenv.2020.144284.
[20] J.M. Chimenos, A.I. Fernández, G. Villalba, M. Segarra, A. Urruticoechea, B. Artaza, F. Espiell, Removal of ammonium and phosphates from wastewater resulting from the process of cochineal extraction using MgO-containing by-product, Water Res. 37 (2003) 1601–1607, https://doi.org/10.1016/S0043-1354(02)00526-2.
[21] M.S. Romero-Güiza, S. Tait, S. Astals, R. del Valle-Zermeño, M. Martínez, J. Mata-Alvarez, J.M. Chimenos, Reagent use efficiency with removal of nitrogen from pig slurry via struvite: a study on magnesium oxide and related by-products, Water Res. 84 (2015) 286–294, https://doi.org/10.1016/j.watres.2015.07.043.
[22] S. Ghosh, S. Lobanov, V.K. Lo, An overview of technologies to recover phosphorus as struvite from wastewater: advantages and shortcomings, Environ. Sci. Pollut. Res 26 (2019) 19063–19077, https://doi.org/10.1007/s11356-019-05378-6.
[23] P. Battistoni, A. De Angelis, P. Pavan, M. Prisciandaro, F. Cecchi, Phosphorus removal from a real anaerobic supernatant by struvite crystallization, Water Res. 35 (2001) 2167–2178, https://doi.org/10.1016/S0043-1354(00)00498-X.
[24] D. Crutchik, N. Morales, J.R. Vázquez-Padín, J.M. Garrido, Enhancement of struvite pellets crystallization in a full-scale plant using an industrial grade magnesium product, Water Sci. Technol. 75 (2017) 609–618, https://doi.org/10.2166/wst.2016.527.
[25] M. Fromberg, M. Pawlik, D.S. Mavinic, Induction time and zeta potential study of nucleating and growing struvite crystals for phosphorus recovery improvements within fluidized bed reactors, Powder Technol. 360 (2020) 715–730, https://doi.org/10.1016/j.powtec.2019.09.067.
[26] M.K.L.N. Sikosana, D.G. Randall, H. Von Blottnitz, A technological and economic exploration of phosphate recovery from centralised sewage treatment in a transitioning economy context, WSA 43 (2017) 343, https://doi.org/10.4314/wsa.v43i2.17.
[27] S. Ghosh, S. Lobanov, V.K. Lo, Investigation of the impact of hydrodynamic parameters for phosphorus recovery from synthetic anaerobic digester supernatant in a fluidized bed reactor, Chem. Eng. Process. - Process. Intensif. 157 (2020) 108155, https://doi.org/10.1016/j.cep.2020.108155.
[28] R. del Valle-Zermeño, J. Formosa, J. Gómez-Manrique, J.M. Chimenos, Desulfurization performance of MgO byproducts as a function of particle size, Energy Fuels 30 (2016) 2328–2335, https://doi.org/10.1021/acs.energyfuels.6b00041.
[29] P. Stolzenburg, A. Capdevielle, S. Teychené, B. Biscans, Struvite precipitation with MgO as a precursor: application to wastewater treatment, Chem. Eng. Sci. 133 (2015) 9–15, https://doi.org/10.1016/j.ces.2015.03.008.
[30] E. Ariyanto, The influence of various physico-chemical process parameters on kinetics and growth mechanism of struvite crystallisation, Adv. Powder Technol. 13 (2014).
[31] M. Shariati-Rad, S. Heidari, Classification and determination of total hardness of water using silver nanoparticles, Talanta 219 (2020) 121297, https://doi.org/10.1016/j.talanta.2020.121297.
[32] N. Park, H. Chang, Y. Jang, H. Lim, J. Jung, W. Kim, Prediction of adequate pH and Mg 2 + dosage using an empirical MgO solubility model for struvite crystallization, Environ. Technol. Innov. 21 (2021) 101347, https://doi.org/10.1016/j.eti.2020.101347.
[33] P. Raschman, A. Fedoročková, Dissolution of periclase in excess of hydrochloric acid: study of inhibiting effect of acid concentration on the dissolution rate, Chem. Eng. J. 117 (2006) 205–211, https://doi.org/10.1016/j.cej.2005.12.019.
[34] J. Bugajski, H. Gamsjäger, Dissolution kinetics of MgO in aqueous, acidic media, Mon. Chem. 117 (1986) 763–772, https://doi.org/10.1007/BF00810067.
[35] M.I.H. Bhuiyan, D.S. Mavinic, F.A. Koch, Thermal decomposition of struvite and its phase transition, Chemosphere 70 (2008) 1347–1356, https://doi.org/10.1016/j.chemosphere.2007.09.056.
[36] Y. Chen, J. Tang, W. Li, Z. Zhong, J. Yin, Thermal decomposition of magnesium ammonium phosphate and adsorption properties of its pyrolysis products toward ammonia nitrogen, Trans. Nonferrous Met. Soc. China 25 (2015) 497–503, https://doi.org/10.1016/S1003-6326(15)63630-5.
[37] L. Bianchi, K. Kirwan, L. Alibardi, M. Pidou, S.R. Coles, Recovery of ammonia from wastewater through chemical precipitation: investigating the kinetic mechanism and reactions pathway of struvite decomposition, J. Therm. Anal. Calor. 142 (2020) 1303–1314, https://doi.org/10.1007/s10973-019-09108-5.
[38] B. Tansel, G. Lunn, O. Monje, Struvite formation and decomposition characteristics for ammonia and phosphorus recovery: a review of magnesium-ammonia-phosphate interactions, Chemosphere 194 (2018) 504–514, https://doi.org/10.1016/j.chemosphere.2017.12.004.
[39] S. Vinardell, Co-digestion of sewage sludge and food waste in a wastewater treatment plant based on mainstream anaerobic membrane bioreactor technology: a techno-economic evaluation, Bioresour. Technol. 11 (2021).
[40] E. Desmidt, K. Ghyselbrecht, A. Monballiu, K. Rabaey, W. Verstraete, B. D. Meesschaert, Factors influencing urease driven struvite precipitation, Sep. Purif. Technol. 110 (2013) 150–157, https://doi.org/10.1016/j.seppur.2013.03.010.
[41] A. Korchef, H. Saidou, M.B. Amor, Phosphate recovery through struvite precipitation by CO2 removal: effect of magnesium, phosphate and ammonium concentrations, J. Hazard. Mater. 186 (2011) 602–613, https://doi.org/10.1016/j.jhazmat.2010.11.045.
[42] D.D. Macdonald, D. Owen, The dissolution of magnesium oxide in dilute sulfuric acid, Can. J. Chem. 49 (1971) 3375–3380, https://doi.org/10.1139/v71-561.
[43] E. Tarragó, S. Puig, M. Ruscalleda, M.D. Balaguer, J. Colprim, Controlling struvite particles' size using the up-flow velocity, Chem. Eng. J. 302 (2016) 819–827, https://doi.org/10.1016/j.cej.2016.06.036.
[44] B. Elduayen-Echave, M. Azcona, P. Grau, P.A. Schneider, Effect of the shear rate and supersaturation on the nucleation and growth of struvite in batch stirred tank reactors, J. Water Process Eng. 38 (2020) 101657.